
Mixed Diffusion for 3D Indoor Scene Synthesis

Siyi Hu¹ Diego Martin Arroyo² Stephanie Debats² Fabian Manhardt²

Luca Carlone¹

Federico Tombari^{2,3}

¹Massachusetts Institute of Technology ²Google, Inc ³Technische Universität München
{siyi, lcarlone}@mit.edu
{martinarroyo, sdebats, fabianmanhardt, tombari}@google.com

Abstract

Realistic conditional 3D scene synthesis significantly enhances and accelerates the creation of virtual environments, which can also provide extensive training data for computer vision and robotics research among other applications. Diffusion models have shown great performance in related applications, *e.g.*, making precise arrangements of unordered sets. However, these models have not been fully explored in floor-conditioned scene synthesis problems. We present MiDiffusion, a novel mixed discrete-continuous diffusion model architecture, designed to synthesize plausible 3D indoor scenes from given room types, floor plans, and potentially pre-existing objects. We represent a scene layout by a 2D floor plan and a set of objects, each defined by its category, location, size, and orientation. Our approach uniquely implements structured corruption across the mixed discrete semantic and continuous geometric domains, resulting in a better conditioned problem for the reverse denoising step. We evaluate our approach on the 3D-FRONT dataset. Our experimental results demonstrate that MiDiffusion substantially outperforms state-of-the-art autoregressive and diffusion models in floor-conditioned 3D scene synthesis. In addition, our models can handle partial object constraints via a corruption-and-masking strategy without task specific training. We show MiDiffusion maintains clear advantages over existing approaches in scene completion and furniture arrangement experiments.

1 Introduction

Generating diverse and realistic 3D indoor scenes has attracted extensive research in computer vision and graphics. In recent years, this problem has been largely motivated by interior designs of apartments and houses, as well as automatic 3D virtual environment creation for video games and data-driven 3D learning tasks [25, 50, 8, 51].

We focus on object-based 3D indoor scene synthesis in which the goal is to predict a set of objects characterized by semantic labels and geometric arrangements. Results using state-of-the-art autoregressive models show that, while it is relatively easy to predict reasonable object labels given a room type, the main bottleneck is generating accurate geometric arrangements of objects, *i.e.*, predicting realistic positions and orientations. Autoregressive models might fail because they cannot revert a bad prediction in an earlier previous step. Therefore, “de-noising” approaches that iteratively refine predicted results are better suited for this type of problems [46].

In this work, we propose to adopt diffusion models [35] for this problem, as the iterative denoising scheme is well suited for improving object geometry in 3D scenes. Denoising Diffusion Probabilistic Models (DDPM) [15] proposed Gaussian corruption and denoising of continuous domain data, resulting in efficient training of diffusion models for image synthesis tasks. Discrete Denoising

Diffusion Probabilistic Models (D3PM) [2] extended the pioneering work of Hoogeboom *et al.* [16] to structured categorical corruption processes for data in discrete state space. Unlike continuous diffusion models, discrete diffusion involves data corruption and recovery using transition probabilities between discrete states. Since object attributes are naturally defined on both discrete and continuous domains, we propose to combine these approaches to form a mixed discrete-continuous diffusion model for 3D scene synthesis problems.

There are a few recent works adopting diffusion models or iterative denoising strategies for 3D scene synthesis problems [17, 13, 46, 41]. The closest work to ours is DiffuScene [41], which generates 3D indoor scenes without floor plan constraints using DDPM by first converting semantic labels to one-hot encoding vectors in the continuous domain and then using argmax to retrieve label predictions. We instead focus on floor-conditioned problems, as these are more practical setups in automatic design of real or virtual worlds. We present three technical contributions in this paper:

- We propose MiDiffusion, a novel mixed discrete-continuous diffusion model combining DDPM and D3PM to iteratively denoise objects’ semantic and geometric attributes which are naturally defined in discrete and continuous domains, respectively.
- We design a time variant transformer-based denoising network with floor plan features as condition vectors for our mixed diffusion approach.
- For applications with partial object constraints, such as scene completion given existing objects, we propose a corruption-and-masking strategy to handle known object conditions without the need to re-train the models.

We compare MiDiffusion against state-of-the-art autoregressive and diffusion models in floor-conditioned 3D scene synthesis problems. Experimental evaluation using the common 3D-FRONT [9] dataset demonstrates that our approach generates more realistic scene layouts, outperforming existing methods. We provide ablation studies supporting our design of the mixed diffusion model and the denoising network. Without re-training, we also show experimental evaluations on scene completion and furniture arrangement, confirming that our approach maintains superior performance on larger scenes. Code and data are available at <https://github.com/MIT-SPARK/MiDiffusion>.

2 Related Works

3D Scene Synthesis. 3D scene synthesis is typically achieved by generating a set of object layouts from scratch. Classical approaches in the computer graphics community typically employ procedural modeling to apply a set of functions that capture object relationships in indoor [50, 25, 49, 32] and outdoor [40, 25, 49, 29, 18, 5] settings. A handful of methods are based on graph representations of the scene. Meta-Sim [18] and Meta-Sim2 [5] learn to modify attributes of scene graphs obtained from probabilistic scene grammars to match synthesized and target images. SG-VAE [30] learns a grammar-based auto-encoder to capture relationships and decode the latent space to a parse tree. Most recently, it is common to learn inter-object relationships implicitly without specifying hand-crafted rules. Existing models include feed-forward networks [53], VAEs [30, 47], GANs [48], and autoregressive models [32, 33, 43, 23, 53, 54, 27, 44, 28]. The state-of-the-art autoregressive models [44, 28] are built with a transformer [42] backbone, capable of well modelling object interactions.

Diffusion Models. Diffusion probabilistic models [38, 15, 2, 26, 36] are generative models defined by two Markov processes. The forward process slowly injects random noise to the data, whereas the reverse denoising process recovers the data. Conceptually, this approach has connections with denoising score matching methods [37, 39]. Following the pioneering work by [35], diffusion models first gained popularity in 2D image synthesis [19, 36], outperforming existing works [20, 6]. Starting from Denoising Diffusion Probabilistic Models (DDPM), diffusion models typically work with latent variables in the continuous domain. However, it is more natural to represent discrete variables, such as text, in discrete state space. Discrete diffusion models were first applied to text generation in argmax flow [16], and then Diffusion Probabilistic Models (D3PMs) [2] and VQ-Diffusion [11] showed strong results on character level image generation and text-to-image synthesis.

Diffusion Models for Layout Synthesis. Very recently, diffusion models became popular for layout synthesis, including document layout generation [17, 13], 3D scene synthesis [41], furniture re-arrangement [46, 41], graph-conditioned 3D layout generation [52, 24], and text conditioned scene synthesis [7]. LayoutDM [17] applies diffusion models in discrete state space. After discretizing position and size to a fixed number of bins, they use the discrete corruption process by VQ-Diffusion [11] to train the reverse transformer network for predicting category, position, and

size for document layout generation. Most related to ours, DiffuScene [41] predicts 3D scene layout using DDPM after converting semantic labels to one-hot encodings to allow joint diffusion with geometric attributes in the continuous domain. In contrast, our diffusion model works directly on the mixed discrete-continuous domains. Moreover, we design a novel corruption-and-masking strategy for reverse diffusion under partial object constraints, without the need to re-train any models.

3 Preliminary: Diffusion Models

Diffusion models [35] typically consist of two Markov processes: a forward corruption process and a reverse denoising process. The forward process $q(\mathbf{x}_{1:T}|\mathbf{x}_0) = \prod_{t=1}^T q(\mathbf{x}_t|\mathbf{x}_{t-1})$ typically corrupts the data $\mathbf{x}_0 \sim q(\mathbf{x}_0)$ into a sequence of latent variables $\mathbf{x}_{1:T}$ by iteratively injecting controlled noise. The reverse process $p_\theta(\mathbf{x}_{0:T}) = p(\mathbf{x}_T) \prod_{t=1}^T p_\theta(\mathbf{x}_{t-1}|\mathbf{x}_t)$ progressively denoises the latent variables via a learned denoising network θ . The standard approach to train the denoising network is to minimize the variational bound on the negative log-likelihood:

$$\mathbb{E}_{q(\mathbf{x}_0)}[-\log p_\theta(\mathbf{x}_0)] \leq \mathbb{E}_{q(\mathbf{x}_{0:T})} \left[-\log \frac{p_\theta(\mathbf{x}_{0:T})}{q(\mathbf{x}_{1:T}|\mathbf{x}_0)} \right] =: L_{vb} \quad (1)$$

which can be re-arranged to

$$\begin{aligned} L_{vb} = & \mathbb{E}_{q(\mathbf{x}_0)} \left[\underbrace{D_{\text{KL}}(q(\mathbf{x}_T|\mathbf{x}_0)||p(\mathbf{x}_T))}_{L_T} + \sum_{t=2}^T \underbrace{\mathbb{E}_{q(\mathbf{x}_t|\mathbf{x}_0)} [D_{\text{KL}}(q(\mathbf{x}_{t-1}|\mathbf{x}_t, \mathbf{x}_0)||p_\theta(\mathbf{x}_{t-1}|\mathbf{x}_t))]}_{L_{t-1}} \right] \\ & + \underbrace{\mathbb{E}_{q(\mathbf{x}_1|\mathbf{x}_0)} [-\log p_\theta(\mathbf{x}_0|\mathbf{x}_1)]}_{L_0}. \end{aligned} \quad (2)$$

If the forward process injects known noise, the approximate posterior q has no learnable parameters and hence L_T can be ignored. Then, efficient learning of network θ requires: (1) efficient sampling of \mathbf{x}_t from $q(\mathbf{x}_t|\mathbf{x}_0)$; and (2) tractable computation of $q(\mathbf{x}_{t-1}|\mathbf{x}_t, \mathbf{x}_0)$.

Diffusion models also apply to conditional synthesis problems, such as text conditioned image generation [15, 2]. Given a conditional input \mathbf{y} , we can write the reverse process as $p_\theta(\mathbf{x}_{0:T}|\mathbf{y}) = p(\mathbf{x}_T) \prod_{t=1}^T p_\theta(\mathbf{x}_{t-1}|\mathbf{x}_t, \mathbf{y})$ and substitute $p_\theta(\mathbf{x}_{t-1}|\mathbf{x}_t)$ by $p_\theta(\mathbf{x}_{t-1}|\mathbf{x}_t, \mathbf{y})$ in Eq. (2). We drop \mathbf{y} in the remainder of this section for simplicity.

Continuous State Space. Denoising Diffusion Probabilistic Model (DDPM) [15] injects Gaussian noise to a continuous state variable \mathbf{x}_0 with fixed variance schedule $\beta_1, \dots, \beta_T \in (0, 1)$:

$$q(\mathbf{x}_t|\mathbf{x}_{t-1}) := \mathcal{N}(\mathbf{x}_t; \sqrt{1 - \beta_t}\mathbf{x}_{t-1}, \beta_t\mathbf{I}). \quad (3)$$

Therefore, there is a closed form expression for sampling \mathbf{x}_t given \mathbf{x}_0 at any time t :

$$q(\mathbf{x}_t|\mathbf{x}_0) = \mathcal{N}(\mathbf{x}_t; \sqrt{\bar{\alpha}_t}\mathbf{x}_0, (1 - \bar{\alpha}_t)\mathbf{I}), \quad (4)$$

where $\alpha_t := 1 - \beta_t$ and $\bar{\alpha}_t := \prod_{s=1}^t \alpha_s$. The forward process posteriors are also tractable when conditioned on \mathbf{x}_0 :

$$q(\mathbf{x}_{t-1}|\mathbf{x}_t, \mathbf{x}_0) = \mathcal{N}(\mathbf{x}_{t-1}; \tilde{\boldsymbol{\mu}}_t(\mathbf{x}_t, \mathbf{x}_0), \tilde{\beta}_t\mathbf{I}), \quad (5)$$

where $\tilde{\boldsymbol{\mu}}_t(\mathbf{x}_t, \mathbf{x}_0) := \frac{\sqrt{\bar{\alpha}_{t-1}}\beta_t}{1-\bar{\alpha}_t}\mathbf{x}_0 + \frac{\sqrt{\bar{\alpha}_t}(1-\bar{\alpha}_{t-1})}{1-\bar{\alpha}_t}\mathbf{x}_t$ and $\tilde{\beta}_t := \frac{1-\bar{\alpha}_{t-1}}{1-\bar{\alpha}_t}\beta_t$. To best approximate Eq. (5), the reverse distributions are Gaussian as well:

$$p_\theta(\mathbf{x}_{t-1}|\mathbf{x}_t) = \mathcal{N}(\mathbf{x}_{t-1}; \boldsymbol{\mu}_\theta(\mathbf{x}_t, t), \boldsymbol{\Sigma}_\theta(\mathbf{x}_t, t)). \quad (6)$$

In practice, the covariance $\boldsymbol{\Sigma}_\theta(\mathbf{x}_t, t) = \sigma^2\mathbf{I}$ can be learned, or fixed to $\sigma^2 = \tilde{\beta}_t$ or $\sigma^2 = \beta_t$.

Discrete State Space. For discrete data, such as semantic labels, it is more natural to define corruption in the discrete domain. We denote a scalar discrete variable with K categories by $z \in \mathbb{Z}^K$ and use $\mathbf{v}(z_t) \in \{0, 1\}^K$ to represent its one-hot encoding. The variational bound over continuous vector \mathbf{x} in Eq. (2) also holds for z . For multi-dimensional z , training loss is summed over all elements. Then the forward process at time t is defined by a transition probability matrix \mathbf{Q}_t , with $[\mathbf{Q}_t]_{mn} = q(z_t = m | z_{t-1} = n)$. The categorical distribution over z_t given z_{t-1} is

$$q(z_t|z_{t-1}) := \text{Cat}(z_t; p = \mathbf{Q}_t\mathbf{v}(z_{t-1})) = \mathbf{v}(z_t)^\top \mathbf{Q}_t\mathbf{v}(z_{t-1}). \quad (7)$$

With the Markov property, we can derive

$$q(z_t|z_0) = \mathbf{v}(z_t)^\top \bar{\mathbf{Q}}_t \mathbf{v}(z_0) \quad (8)$$

$$q(z_{t-1}|z_t, z_0) = \frac{(\mathbf{v}(z_t)^\top \mathbf{Q}_t \mathbf{v}(z_{t-1})) (\mathbf{v}(z_{t-1})^\top \bar{\mathbf{Q}}_{t-1} \mathbf{v}(z_0))}{\mathbf{v}(z_t)^\top \bar{\mathbf{Q}}_t \mathbf{v}(z_0)} \quad (9)$$

where $\bar{\mathbf{Q}}_t = \mathbf{Q}_t \mathbf{Q}_{t-1} \cdots \mathbf{Q}_1$. The denoising network θ is trained to compute the categorical distributions $p_\theta(z_{t-1}|z_t)$. We implement the mask-and-replace strategy by VQ-Diffusion [11], which improves upon the proposed choices of \mathbf{Q}_t in [2] by introducing an additional special token [MASK].

4 3D Scene Synthesis via Mixed Diffusion

We present MiDiffusion, a mixed discrete-continuous diffusion model for 3D indoor scene synthesis. We assume each scene \mathcal{S} is in a world frame with the origin at the center. It consists of a floor plan and at most N objects. We denote the floor plan by a conditional vector \mathbf{y} . Each object in the scene is characterized by its semantic label $z \in \{1, 2, \dots, C\}$, centroid position $\mathbf{t} \in \mathbb{R}^3$, bounding box size $\mathbf{s} \in \mathbb{R}^3$, and rotation angle around the vertical axis $\phi \in SO(2)$. Inspired by LEGO-Net [46], we represent ϕ as $[\cos(\gamma), \sin(\gamma)]^\top$ to maintain continuity on $SO(2)$ [55]. We concatenate all geometric attributes to $\mathbf{x} = (\mathbf{t}, \mathbf{s}, \phi)$. Then, we can represent a 3D indoor scene as $\mathcal{S} = (\{(z^i, \mathbf{x}^i)\}_{1 \leq i \leq N}, \mathbf{y})$. We designate the last semantic label $z = C$ to an ‘‘empty’’ label to work with scenes containing less than N objects and define geometric attributes to all zeros for an ‘‘empty’’ object.

The problem of synthesising 3D scenes can be viewed as learning a network θ that maximizes $\log p_\theta(z_0^i, \mathbf{x}_0^i | \mathbf{y})$ over all objects and across all scenes, *i.e.*, the same variational bound in Eq. (2) but over two domains. We drop the superscript i for simplicity.

4.1 Diffusion in Mixed Discrete-Continuous Domains

Although object semantic and geometric attributes are in separate domains, we define a corruption process in MiDiffusion that independently injects domain-specific noises to z_t and \mathbf{x}_t as in D3PM and DDPM, respectively:

$$q(z_t, \mathbf{x}_t | z_{t-1}, \mathbf{x}_{t-1}) := \tilde{q}(z_t | z_{t-1}) \cdot \hat{q}(\mathbf{x}_t | \mathbf{x}_{t-1}). \quad (10)$$

This means we can sample z_t, \mathbf{x}_t independently in training, and factor the posterior distribution as

$$q(z_{t-1}, \mathbf{x}_{t-1} | z_t, \mathbf{x}_t, z_0, \mathbf{x}_0) = \tilde{q}(z_{t-1} | z_t, z_0) \cdot \hat{q}(\mathbf{x}_{t-1} | \mathbf{x}_t, \mathbf{x}_0). \quad (11)$$

In the backward diffusion process, we can design a network θ that computes probability distributions over latent variables by domains to be consistent with the forward process:

$$p_\theta(z_{t-1}, \mathbf{x}_{t-1} | z_t, \mathbf{x}_t, \mathbf{y}) := \tilde{p}_\theta(z_{t-1} | z_t, \mathbf{x}_t, \mathbf{y}) \cdot \hat{p}_\theta(\mathbf{x}_{t-1} | \mathbf{x}_t, z_t, \mathbf{y}). \quad (12)$$

Note that the general loss function to train diffusion models in Eq. (2) consists of two types: $\{L_{t-1}\}_{2 \leq t \leq T}$, the KL-divergence terms, and L_0 , a negative log probability. The factorization in Eq. (10) to (12) allows us to re-arrange these terms to a pair of domain specific losses:

$$\begin{aligned} L_{t-1}^{mixed} &= \mathbb{E}_{q(z_t, \mathbf{x}_t | z_0, \mathbf{x}_0)} [D_{\text{KL}}(q(z_{t-1}, \mathbf{x}_{t-1} | z_t, \mathbf{x}_t, z_0, \mathbf{x}_0) || p_\theta(z_{t-1}, \mathbf{x}_{t-1} | z_t, \mathbf{x}_t, \mathbf{y})))] \\ &= \underbrace{\mathbb{E}_{\tilde{q}(z_t | z_0)} [D_{\text{KL}}(\tilde{q}(z_{t-1} | z_t, z_0) || \tilde{p}_\theta(z_{t-1} | z_t, \mathbf{x}_t, \mathbf{y}))]}_{L_{t-1}^{D3PM}} \\ &\quad + \underbrace{\mathbb{E}_{\hat{q}(\mathbf{x}_t | \mathbf{x}_0)} [D_{\text{KL}}(\hat{q}(\mathbf{x}_{t-1} | \mathbf{x}_t, \mathbf{x}_0) || \hat{p}_\theta(\mathbf{x}_{t-1} | \mathbf{x}_t, z_t, \mathbf{y}))]}_{L_{t-1}^{DDPM}}, \end{aligned} \quad (13)$$

$$\begin{aligned} L_0^{mixed} &= \mathbb{E}_{q(z_1, \mathbf{x}_1 | z_0, \mathbf{x}_0)} [-\log p_\theta(z_0, \mathbf{x}_0 | z_1, \mathbf{x}_1, \mathbf{y})] \\ &= \underbrace{\mathbb{E}_{\tilde{q}(z_1 | z_0)} [-\log \tilde{p}_\theta(z_0 | z_1, \mathbf{x}_1, \mathbf{y})]}_{L_0^{D3PM}} + \underbrace{\mathbb{E}_{\hat{q}(\mathbf{x}_1 | \mathbf{x}_0)} [-\log \hat{p}_\theta(\mathbf{x}_0 | \mathbf{x}_1, z_1, \mathbf{y})]}_{L_0^{DDPM}}. \end{aligned} \quad (14)$$

Since $(\mathbf{x}_t, \mathbf{y})$ is the joint condition term in the reverse step p_θ to predict z_{t-1} , the first term in Eq. (13) matches exactly L_{t-1} in D3PM. Similarly, the second term matches L_{t-1} in DDPM. The

factorization in Eq. (14) is similar to that in Eq. (13). We provide more details about the factorization step in Eq. (13) in Appendix B.

Combining Eq. (13), (14), we get the exact sum of variational bounds in D3PM and DDPM. Intuitively, summing over discrete and continuous losses is similar to summing losses over each coordinate given multi-dimensional data in vanilla DDPM or D3PM. We use a simplified version of L_{vb}^{DDPM} after re-parameterizing the forward process as suggested in DPPM to improve training stability and efficiency. We add an auxiliary loss, L_{aux}^{D3PM} , as proposed in D3PM to encourage good predictions for z_0 at each time step. We include re-parameterization steps as suggested by DDPM and D3PM in Appendix A. The combined loss for MiDiffusion is:

$$L^{mixed} = L_{vb}^{DDPM} + L_{vb}^{D3PM} + \lambda L_{aux}^{D3PM}. \quad (15)$$

4.2 Denoising Network

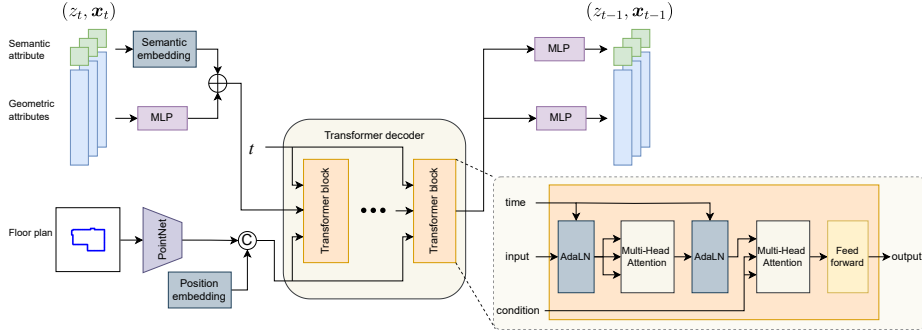


Figure 1: **Denoising network.** The time-variant decoder backbone takes object features as input, conditioned by the floor plan feature after concatenation with positional embeddings of object indices. We utilize the time-variant transformer decoder block from VQ-Diffusion [11].

We use a transformer-based denoising network as shown in Fig. 1, which takes in latent variables (z_t, \mathbf{x}_t) at step t and predicts the categorical distribution $p_\theta(z_{t-1}|z_t, \mathbf{x}_t, \mathbf{y})$, together with the Gaussian mean of $p_\theta(\mathbf{x}_{t-1}|\mathbf{x}_t, z_t, \mathbf{y})$ assuming a fixed covariance. At test time, we can simply sample from these distributions to retrieve $(z_{t-1}, \mathbf{x}_{t-1})$.

Feature encoder. We encode the object features by passing geometric attributes through an MLP and combine them with trainable semantic embeddings. For each scene, we sample 256 points from a floor plan image along the boundary and compute outward normal vectors. We use the PointNet [31] floor plan feature extractor from LEGO-Net [46] as it is more lightweight and better captures floor boundary than image-based feature extractors. The floor plan feature is then concatenated with the learned position embedding, which is commonly used in transformer architectures, to form the conditioning vector.

Transformer decoder. The backbone of our denoising network is a time-variant transformer decoder adapted from VQ-Diffusion [11]. We show in experimentally that the multi-head attention mechanism in the transformer decoder better captures boundary constraints than the conditional 1-D U-Net [34] architecture proposed in DiffuScene [41]. We show our denoising network in Fig. 1. Within each transformer block, the time step is injected through the Adaptive Layer Normalization (AdaLN) [3] operator. The conditioning inputs are sent through a multi-head cross-attention layer.

Feature extractor. We feed the output of the transformer decoder to two MLPs to generate categorical distribution for p_θ and Gaussian means for the geometric features.

4.3 Partial Condition on Objects

3D scene synthesis is sometimes constrained by known object information, such as scene completion given existing objects. DiffuScene [41] considers these as additional condition inputs to the denoising network, which requires at least a task-specific feature encoder for the condition inputs and hence re-training of the entire model. We instead propose to address this flexibility issue through a corruption-and-masking strategy which does not require any additional training. Since the core idea of diffusion models is to recover real data by learning the inverse of a known corruption process, we can force the constrained sections of the latent variables to follow exactly the inverse of the controlled

corruption steps in the denoising process. For example, for scene completion: given M objects, we first compute a sequence of latent variables $\{(z_t^i, \mathbf{x}_t^i)\}_{1 \leq i \leq M}$ through the corruption process. This allows us to mask out the first M objects using pre-computed latent variables at time t in the reverse process. These latent variables eventually converge to the known input $\{(z_0^i, \mathbf{x}_0^i)\}_{1 \leq i \leq M}$ without additional training. This strategy can generalize to other applications, such as furniture arrangement and label conditioned scene synthesis, by targeting different sections of latent object variables.

5 Experimental Evaluation

In this section, we present evaluation results comparing MiDiffusion against existing methods and provide ablation studies. We also show that, without re-training, our models can be applied to other tasks such as scene completion and furniture arrangement. Additional results and implementation details can be found in the appendix.

Dataset. We use the common benchmarking dataset, 3D-FRONT [9], for evaluation. This is a synthetic dataset of 18,797 rooms furnished by 7,302 textured objects from 3D-FUTURE [10]. We evaluate on three room types: 4041 bedrooms, 900 dining rooms, and 813 living rooms. We use the same data processing and training/testing data split as [28]. We use rotation augmentations in 90° increments during training as in [41] to be consistent with the baselines.

Baselines. We compare our proposed approaches against two state-of-the-art 3D scene synthesis methods: (1) ATISS [28], an autoregressive model with a transformer encoder backbone that generates sequential predictions of objects; (2) DiffuScene [41], a diffusion model with a conditional 1D U-Net [34] denoising backbone based on DDPM. We train baseline models with their open-source code and default hyper parameters. We compare MiDiffusion with DiffuScene in its original application, *i.e.*, unconditioned scene synthesis, in Appendix E.2.

Implementation. We train all our models with the Adam optimizer [21] at $l_r = 2e^{-4}$ with a 0.5 decay rate every $10k$ for $50k$ epochs on the bedroom dataset, and every $15k$ epochs for $10k$ epochs on the dining room and living room datasets. We set $\lambda = 0.05$ for the auxiliary loss term L_{aux}^{D3PM} . More details about implementation and network parameters are included in Appendix C.

Evaluation Metrics. We randomly select 1000 floor plans from the test set as input and evaluate models using metrics found in prior works [44, 28, 41]: KL divergence of object label distributions ($KL \times 0.01$), Fréchet inception distance (FID), Kernel inception distance ($KID \times 0.001$), and classification accuracy (CA%) using the implementation by ATISS. While the KL divergence evaluates the predicted object label distributions, the other metrics are used to compare the layout images with the ground-truth test data. We render each scene to a 256×256 top-down orthographic projection image using CAD models from 3D-FUTURE. In line with DiffuScene, we color each object according to its semantic class. We render bedrooms to 6.1m squares, and the living and dining rooms to 12.2m squares. Appendix D includes example layout images. We report CA % over 10 runs with random sampling of predicted layouts for training and testing. Note that realistic layouts should have a low FID/KID, a low KL and a CA% that is close to 50%. We also compute additional metrics, averaged over all scenes to further evaluate object placement, including the number of generated objects (Obj), percentage of out-of-boundary objects (OOB %), and bounding box Intersection over Union (IoU %). We dilate the room boundary by 0.1m for OOB % computation to account for slight under estimation of floor boundary in the raw 3D-FRONT data.

5.1 Floor Plan Conditioned 3D Scene Synthesis

We first compare MiDiffusion against baselines in floor-conditioned 3D scene synthesis experiments without existing objects. Fig. 2 include qualitative results rendered in PyVista. The object mesh is retrieved from the 3D-FUTURE [10] dataset by finding the closest match in size under the predicted semantic category. We replace original textures in the CAD models by label specific color for clarity. We include examples of orthographic projection images, which we use for quantitative evaluations, in the appendix. In general, our approach is able to generate realistic object arrangement whilst respecting the boundary constraints. ATISS generates slightly less precise object placement compared to the two diffusion based approaches, *e.g.*, the table-chairs furniture set in the last example of Fig. 2 is not exactly symmetric. Both DiffuScene and ATISS show higher tendency to place objects outside the floor boundary than ours. This problem is more prominent for DiffuScene, most likely due to the conditional U-Net architecture in their denoising network, which does not learn boundary constraints equally well as transformer architectures.

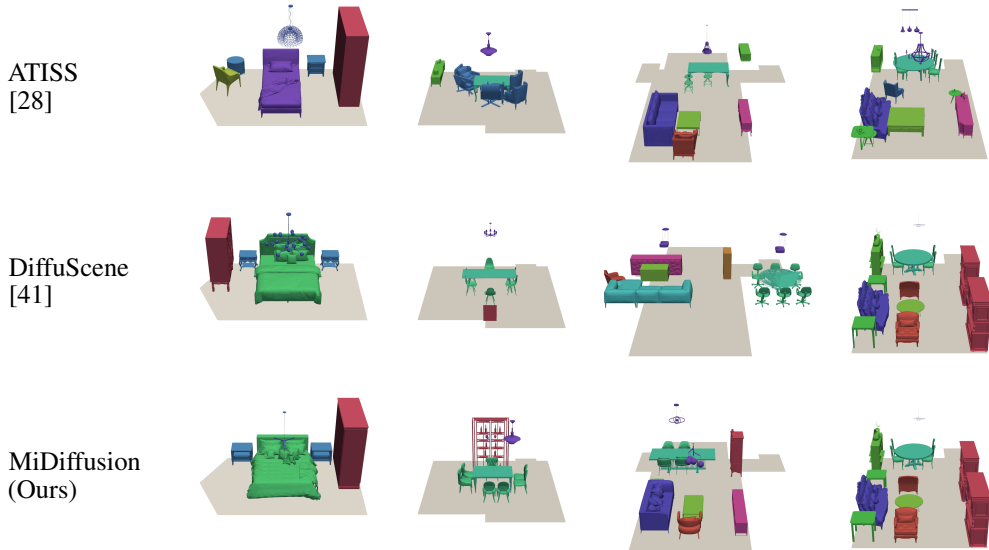


Figure 2: **Floor-conditioned scene synthesis.** The meshes are retrieved from the 3D-FUTURE [10] dataset by size matching within predicted semantic category. MiDiffusion generates realistic arrangements while respecting boundary constraints.

We show quantitative results in Tables 1 and 2. Overall, our approach achieves substantially better performance in generating realistic layouts, especially in the dining room and living room datasets. There are large margins between our models and the baseline models for FID, $KID \times 0.001$ and CA %, comparing images of synthesized layouts. As for object label distributions, there seems to be no large differences between the individual methods with respect to $KL \times 0.01$. In fact, all methods have rather small KL values and the difference could be due to random sampling. In Table 2, there is a trade-off between keeping objects inside the boundary (low OOB%) and maintaining minimal overlap (low IoU%). Although DiffuScene achieves the lowest IoU%, their models tend to place more objects outside the boundary than the others, which explains their sub-optimal performance in Table 1. Overall, our approach is still the best in terms of object placement that are compatible with other predicted objects and the floor boundary constraints.

Method	Bedroom				Dining room				Living room			
	FID	$KID \times 0.001$	CA %	$KL \times 0.01$	FID	$KID \times 0.001$	CA %	$KL \times 0.01$	FID	$KID \times 0.001$	CA %	$KL \times 0.01$
ATISS	65.76	1.21	54.44 ± 3.69	0.94	41.06	10.54	64.06 ± 5.63	1.89	38.03	9.20	63.98 ± 4.60	1.55
DiffuScene	66.45	1.05	58.70 ± 4.93	3.41	45.88	9.30	65.34 ± 6.55	1.55	47.91	11.75	73.96 ± 4.93	1.95
MiDiffusion (Ours)	63.71	0.24	53.65 ± 2.46	1.05	30.63	2.74	52.10 ± 1.72	1.90	28.99	1.60	54.69 ± 1.54	1.54

Table 1: Evaluation results for floor-conditioned 3D scene synthesis.

Method	Bedroom			Dining room			Living room		
	Obj	OOB %	IoU %	Obj	OOB %	IoU %	Obj	OOB %	IoU %
ATISS	5.52	16.26	1.00	11.43	17.43	1.86	13.00	17.39	1.49
DiffuScene	5.05	8.06	0.41	10.90	28.16	0.56	11.79	33.75	0.43
MiDiffusion (Ours)	5.22	3.91	0.61	10.92	5.77	0.91	12.28	8.71	0.69
Ground truth	5.22	3.37	0.24	11.11	0.73	0.48	11.67	1.55	0.27

Table 2: Geometric evaluations for floor-conditioned 3D scene synthesis.

Diversity. We study the diversity of the predicted layouts by measuring the average standard deviation (std) of object centroid positions and bounding box sizes. Since vertical positions are highly correlated with semantic labels, which are already evaluated through KL-divergence, the std over positions is averaged over the two planar axes. The results are in Table 3, where the “IB” suffix means results are computed over “in-boundary” objects only to remove bad object placement. However, these numbers are not directly comparable due to large differences in OOB% across approaches. Nevertheless, our approach generates the most diverse object placements that are within the floorplan boundary (*i.e.*, Position-IB). We are slightly less diverse in sizes (*i.e.*, Size-IB) than DiffuScene, but our approach shows the least drop in size variety after removing out-of-boundary objects.

Ablation study. In Table 4, we study the effect of our mixed-diffusion formulation and PointNet floor plan feature extractor. We provide results of modified versions of MiDiffusion: (1) with DDPM

Method	Bedroom				Dining room				Living room			
	Position	Position-IB	Size	Size-IB	Position	Position-IB	Size	Size-IB	Position	Position-IB	Size	Size-IB
ATISS	1.074	1.035	0.709	0.663	1.586	1.504	0.434	0.385	1.730	1.663	0.442	0.409
DiffuScene	1.073	1.059	0.718	0.691	1.596	1.427	0.454	0.423	1.752	1.575	0.482	0.439
MiDiffusion (Ours)	1.073	1.067	0.698	0.680	1.568	1.558	0.414	0.399	1.670	1.667	0.441	0.427

Table 3: Average std of predicted object positions and sizes for floor-conditioned 3D scene synthesis.

and ResNet-18 [12] as floor plan feature extractor as in ATISS and DiffuScene; (2) with DDPM and PointNet. The last row shows our method MiDiffusion (*i.e.*, using our mixed diffusion formulation together with PointNet). The first variant, DDPM+ResNet is similar to DiffuScene, except we use a transformer based denoising network rather than its U-Net counterpart. Note that the respective results already exceed DiffuScene in Table 1, suggesting that the transformer architecture is better at learning boundary constraints. However, there is a large deterioration in KL divergence. Next, while replacing the ResNet floor feature extractor by a more lightweight PointNet extractor brings a significant performance boost in the dining and living room datasets, which contain less training scenes but are of larger room sizes, the performance decreases on the bedroom dataset. It is likely that PointNet works better under complex and limited training data, but suffers from sampling noise during conversion of the floor plan image to points and normals in the opposite situation. Overall, we achieve the best results with our complete formulation in which the mixed diffusion approach avoids lifting the discrete inputs to a continuous space as required by the DDPM formulation. We include additional geometric evaluation results in Appendix E.1

Method	Bedroom				Dining room				Living room			
	FID	KIDx0.001	CA %	KLx0.01	FID	KIDx0.001	CA %	KLx0.01	FID	KIDx0.001	CA %	KLx0.01
DDPM+ResNet	63.73	0.35	54.86 ± 4.22	4.72	31.35	3.77	53.58 ± 4.06	5.88	30.44	3.05	63.48 ± 6.21	6.06
DDPM+PointNet	65.25	1.25	57.00 ± 4.67	2.14	31.43	2.85	52.71 ± 4.55	2.72	28.63	1.68	55.27 ± 5.44	1.93
Mixed+PointNet	63.71	0.24	53.65 ± 2.46	1.05	30.63	2.74	52.10 ± 1.72	1.90	28.99	1.60	54.69 ± 1.54	1.54

Table 4: Ablation study for floor-conditioned 3D scene synthesis.

5.2 Floor Plan Conditioned 3D Scene Synthesis with Object Constraints

Recall from Sec. 4.3 that we can re-use the same MiDiffusion models for problems involving partial object constraints through a corruption-and-masking strategy. This approach forces the relevant object attributes to follow the reverse of a pre-computed corruption process in the denoising step, without the need of task-specific retraining.

5.2.1 Scene completion

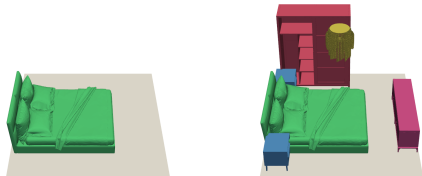


Figure 3: Bedroom completion given a bed.

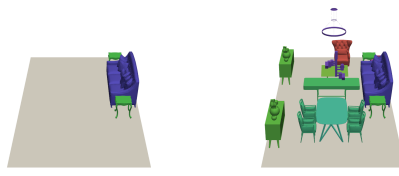


Figure 4: Living room completion given sofa and corner tables.

We first compare our approach with baselines for scene completion (*i.e.*, scene synthesis conditioned on existing objects). We train the DiffuScene-SC variant, which includes an additional module to learn existing object features as a conditional input, using their suggested hyper-parameters and providing 3 existing objects during training. The number of existing objects can be arbitrary at test time. We use the same models for ATISS and MiDiffusion. We use the proposed corruption-and-masking strategy over MiDiffusion models trained in Section 5.1. Fig. 3 shows a simple example of completing a bedroom design that originally only consists of a single bed. Fig. 4 shows another more complex example for completion of a living space. Note that MiDiffusion is able to generate a natural and symmetric set of furniture layout.

We perform quantitative evaluations in Table 5. This is an easier problem for ATISS and DiffuScene than the previous setup. In particular, ATISS is an autoregressive model and therefore existing objects allow the models to skip the first few iterations reducing the chance for mistakes. DiffuScene-SC is, on the other hand, specially designed and trained for this task. Based results in Table 1, these approaches indeed benefit from using existing objects as anchors. Without any retraining, our approach still

outperforms these approaches, when given only 1 existing object. When given 3 objects, our models are still better for the dining room and living room datasets and, however, are outperformed by DiffuScene-SC on the bedroom dataset. Note that the bedroom data has only an average of only 5.22 objects. Therefore, specially trained networks, such as DiffuScene-SC, might be better suited given the very high percentage of pre-existing objects.

Method	Bedroom				Dining room				Living room			
	FID	KID x 0.001	KL x 0.01	OOB %	FID	KID x 0.001	KL x 0.01	OOB %	FID	KID x 0.001	KL x 0.01	OOB %
1 obj												
ATISS	60.59	0.19	1.04	13.52	36.63	7.77	1.79	15.30	34.34	7.15	1.46	16.19
DiffuScene-SC	83.90	19.17	18.34	3.11	34.12	4.82	1.59	12.13	36.32	6.64	1.30	21.74
MiDiffusion (ours)	60.08	-0.03	0.91	3.32	28.56	1.88	1.58	5.29	28.21	1.78	1.47	8.04
3 obj												
ATISS	51.83	-0.57	0.66	8.89	33.53	5.39	1.60	12.26	31.78	5.39	1.43	13.03
DiffuScene-SC	42.77	-1.08	0.80	5.13	30.58	3.67	0.84	10.04	32.07	4.58	0.57	16.13
MiDiffusion (ours)	52.19	-0.32	1.00	4.05	27.60	1.85	1.72	3.97	27.46	1.91	0.95	7.22

Table 5: Evaluation results for scene completion.

5.2.2 Furniture Arrangement

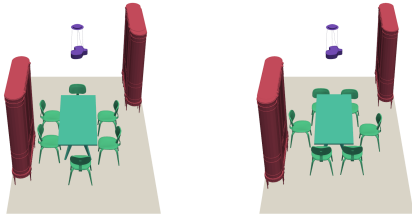


Figure 5: Different table-chair arrangements.

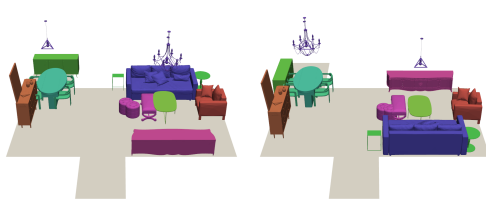


Figure 6: Different living room furniture placement directions.

MiDiffusion can also be used for furniture arrangement, which refers to a scene synthesis problem conditioned on object labels and bounding box sizes without an initial configuration. We use our proposed corruption-and-masking strategy over these attributes to test our models in this setting, and compare the results against DiffuScene’s furniture arrangement variant (DiffuScene-FA). ATISS models are not well suited for this task, since replacing the predicted object label by constraints breaks the stopping condition in their autoregressive pipeline. Fig. 5 shows a simple example of a dining room with two different chair arrangements, as generated by MiDiffusion. Fig. 6 instead illustrates two opposite placements of the living room section given the same inputs. We show quantitative results in Table 6. Without re-training, our models outperform DiffuScene-FA in all metrics.

Method	Bedroom				Dining room				Living room			
	FID	KIDx0.001	OBB %	IoU %	FID	KIDx0.001	OBB %	IoU %	FID	KIDx0.001	OBB %	IoU %
DiffuScene-FA	61.03	0.14	8.03	0.75	33.90	4.14	12.30	1.16	34.62	6.04	17.84	1.31
MiDiffusion (ours)	59.08	-0.24	7.34	0.55	31.72	3.91	6.35	0.96	29.79	3.13	8.33	0.84

Table 6: Evaluation results for furniture arrangement experiment.

5.2.3 Additional Applications

Our models can easily extend to other applications with the right choice of masking. For example, they can be applied to object type conditioned scene synthesis given a list of labels. We can even combine partial constraints on object attributes (*e.g.*, label) with existing objects for constrained scene completion problems. We show qualitative examples in Appendix F.1.

6 Limitations

Though our method shows competitive performance in different layout generation tasks, it has several limitations: the current definition of objects as a collection of bounding box features and labels is not the most precise representation for a 3D setting, and gaining a good understanding of 3D features can potentially improve upon this aspect. In addition, MiDiffusion still requires a model retrieving strategy to compose the final 3D scene configuration. In the future we want to investigate the use of a strong 3D shape priors (*e.g.* in the form of a point cloud or mesh encoder) and integrating mesh and texture synthesis capabilities, similar to SceneTex [4], to enhance realism. Finally, we also plan to investigate how to remove the need for separate models per room.

7 Conclusion

In this work we introduced MiDiffusion, a novel mixed diffusion model combining DDPM and D3PM for object based 3D indoor scene synthesis. This formulation circumvents the need of adopting vector representation of semantic labels in the continuous domain as done in prior works. We designed a denoising architecture that has a time-variant transformer decoder backbone and outputs predictions separately for discrete semantic attributes and continuous geometric attributes. We proposed a unique corruption-and-masking strategy to conduct scene completion and furniture arrangement without the need to re-train our models. We provided extensive experimental evaluation using common benchmarks against state-of-the-art autoregressive and diffusion models. The results show a clear advantage of our approach over the state of the art with or without partial constraints. We also presented ablation studies supporting our design of the mixed diffusion framework as well as the denoising architecture.

References

- [1] Katharopoulos Angelos and Despoina Paschalidou. simple-3dviz. <https://simple-3dviz.com>, 2020.
- [2] Jacob Austin, Daniel D. Johnson, Jonathan Ho, Daniel Tarlow, and Rianne van den Berg. Structured Denoising Diffusion Models in Discrete State-Spaces. In *Advances in Neural Information Processing Systems*, November 2021.
- [3] Jimmy Lei Ba, Jamie Ryan Kiros, and Geoffrey E. Hinton. Layer Normalization, July 2016.
- [4] Dave Zhenyu Chen, Haoxuan Li, Hsin-Ying Lee, Sergey Tulyakov, and Matthias Nießner. Scenetex: High-quality texture synthesis for indoor scenes via diffusion priors, 2023.
- [5] Jeevan Devaranjan, Amlan Kar, and Sanja Fidler. Meta-Sim2: Unsupervised Learning of Scene Structure for Synthetic Data Generation. In Andrea Vedaldi, Horst Bischof, Thomas Brox, and Jan-Michael Frahm, editors, *Computer Vision – ECCV 2020*, volume 12362, pages 715–733. Springer International Publishing, 2020.
- [6] Patrick Esser, Robin Rombach, and Bjorn Ommer. Taming Transformers for High-Resolution Image Synthesis. In *2021 IEEE/CVF Conference on Computer Vision and Pattern Recognition (CVPR)*, pages 12868–12878, Nashville, TN, USA, June 2021. IEEE.
- [7] Weixi Feng, Wanrong Zhu, Tsu-Jui Fu, Varun Jampani, Arjun Reddy Akula, Xuehai He, S. Basu, Xin Eric Wang, and William Yang Wang. LayoutGPT: Compositional Visual Planning and Generation with Large Language Models. In *Conference on Neural Information Processing Systems*, November 2023.
- [8] Matthew Fisher, Manolis Savva, and Pat Hanrahan. Characterizing structural relationships in scenes using graph kernels. In *ACM SIGGRAPH 2011 papers, SIGGRAPH ’11*, pages 1–12. Association for Computing Machinery, July 2011.
- [9] Huan Fu, Bowen Cai, Lin Gao, Ling-Xiao Zhang, Jiaming Wang, Cao Li, Qixun Zeng, Chengyue Sun, Rongfei Jia, Binqiang Zhao, et al. 3d-front: 3d furnished rooms with layouts and semantics. In *Proceedings of the IEEE/CVF International Conference on Computer Vision*, pages 10933–10942, 2021.
- [10] Huan Fu, Rongfei Jia, Lin Gao, Mingming Gong, Binqiang Zhao, Steve Maybank, and Dacheng Tao. 3d-future: 3d furniture shape with texture. *International Journal of Computer Vision*, pages 1–25, 2021.
- [11] Shuyang Gu, Dong Chen, Jianmin Bao, Fang Wen, Bo Zhang, Dongdong Chen, Lu Yuan, and Baining Guo. Vector Quantized Diffusion Model for Text-to-Image Synthesis. In *2022 IEEE/CVF Conference on Computer Vision and Pattern Recognition (CVPR)*, pages 10686–10696. IEEE, 2022.
- [12] Kaiming He, Xiangyu Zhang, Shaoqing Ren, and Jian Sun. Deep residual learning for image recognition. In *2016 IEEE/CVF Conference on Computer Vision and Pattern Recognition (CVPR)*, pages 770–778, 2016.
- [13] Liu He, Yijuan Lu, John Corring, Dinei Florencio, and Cha Zhang. Diffusion-based Document Layout Generation, 2023.
- [14] Dan Hendrycks and Kevin Gimpel. Gaussian Error Linear Units (GELUs), June 2016.

- [15] Jonathan Ho, Ajay Jain, and Pieter Abbeel. Denoising Diffusion Probabilistic Models. In *Advances in Neural Information Processing Systems*, volume 33, pages 6840–6851. Curran Associates, Inc., 2020.
- [16] Emiel Hoogeboom, Didrik Nielsen, Priyank Jaini, Patrick Forré, and Max Welling. Argmax Flows and Multinomial Diffusion: Learning Categorical Distributions. In *Advances in Neural Information Processing Systems*, November 2021.
- [17] Naoto Inoue, Kotaro Kikuchi, Edgar Simo-Serra, Mayu Otani, and Kota Yamaguchi. LayoutDM: Discrete Diffusion Model for Controllable Layout Generation. In *2023 IEEE/CVF Conference on Computer Vision and Pattern Recognition (CVPR)*, pages 10167–10176. IEEE, June 2023.
- [18] Amlan Kar, Aayush Prakash, Ming-Yu Liu, Eric Cameracci, Justin Yuan, Matt Rusiniak, David Acuna, Antonio Torralba, and Sanja Fidler. Meta-Sim: Learning to Generate Synthetic Datasets. In *2019 IEEE/CVF International Conference on Computer Vision (ICCV)*, pages 4550–4559, Seoul, Korea (South), October 2019. IEEE.
- [19] Tero Karras, Timo Aila, Miika Aittala, and Samuli Laine. Elucidating the Design Space of Diffusion-Based Generative Models. In *36th Conference on Neural Information Processing Systems*, 2022.
- [20] Tero Karras, Miika Aittala, Janne Hellsten, Samuli Laine, Jaakko Lehtinen, and Timo Aila. Training Generative Adversarial Networks with Limited Data. In *Advances in Neural Information Processing Systems*, volume 33, pages 12104–12114. Curran Associates, Inc., 2020.
- [21] Diederik P. Kingma and Jimmy Ba. Adam: A method for stochastic optimization. In Yoshua Bengio and Yann LeCun, editors, *3rd International Conference on Learning Representations, ICLR 2015, San Diego, CA, USA, May 7-9, 2015, Conference Track Proceedings*, 2015.
- [22] Alex Krizhevsky, Ilya Sutskever, and Geoffrey E Hinton. ImageNet classification with deep convolutional neural networks. In *Conference on Neural Information Processing Systems*, pages 1097–1105, 2012.
- [23] Manyi Li, Akshay Gadi Patil, Kai Xu, Siddhartha Chaudhuri, Owais Khan, Ariel Shamir, Changhe Tu, Baoquan Chen, Daniel Cohen-Or, and Hao Zhang. GRAINS: Generative Recursive Autoencoders for INdoor Scenes. *ACM Transactions on Graphics*, 38:12:1–12:16, February 2019.
- [24] Chenguo Lin and Yadong Mu. InstructScene: Instruction-Driven 3D Indoor Scene Synthesis with Semantic Graph Prior. In *International Conference on Learning Representations (ICLR)*, February 2024.
- [25] Paul Merrell, Eric Schkufza, Zeyang Li, Maneesh Agrawala, and Vladlen Koltun. Interactive furniture layout using interior design guidelines. In *ACM SIGGRAPH 2011 papers*, SIGGRAPH ’11, pages 1–10. Association for Computing Machinery, July 2011.
- [26] Alexander Quinn Nichol and Prafulla Dhariwal. Improved Denoising Diffusion Probabilistic Models. In *38th International Conference on Machine Learning*, pages 8162–8171. PMLR, July 2021.
- [27] Wamiq Para, Paul Guerrero, Tom Kelly, Leonidas Guibas, and Peter Wonka. Generative Layout Modeling using Constraint Graphs. In *2021 IEEE/CVF International Conference on Computer Vision (ICCV)*, pages 6670–6680. IEEE, October 2021.
- [28] Despoina Paschalidou, Amlan Kar, Maria Shugrina, Karsten Kreis, Andreas Geiger, and Sanja Fidler. ATISS: Autoregressive Transformers for Indoor Scene Synthesis. In *Advances in Neural Information Processing Systems*, volume 34, pages 12013–12026. Curran Associates, Inc., 2021.
- [29] Aayush Prakash, Shaad Boochoon, Mark Brophy, David Acuna, Eric Cameracci, Gavriel State, Omer Shapira, and Stan Birchfield. Structured Domain Randomization: Bridging the Reality Gap by Context-Aware Synthetic Data. In *2019 International Conference on Robotics and Automation (ICRA)*, pages 7249–7255, Montreal, QC, Canada, May 2019. IEEE Press.
- [30] Pulak Purkait, Christopher Zach, and Ian Reid. SG-VAE: Scene Grammar Variational Autoencoder to Generate New Indoor Scenes. In *ECCV*, pages 155–171. Springer International Publishing, 2020.
- [31] Charles R Qi, Hao Su, Kaichun Mo, and Leonidas J Guibas. Pointnet: Deep learning on point sets for 3D classification and segmentation. In *2017 IEEE/CVF Conference on Computer Vision and Pattern Recognition (CVPR)*, pages 652–660, 2017.

- [32] Siyuan Qi, Yixin Zhu, Siyuan Huang, Chenfanfu Jiang, and Song-Chun Zhu. Human-centric Indoor Scene Synthesis Using Stochastic Grammar. In *2018 IEEE/CVF Conference on Computer Vision and Pattern Recognition (CVPR)*. arXiv, August 2018.
- [33] Daniel Ritchie, Kai Wang, and Yu-An Lin. Fast and Flexible Indoor Scene Synthesis via Deep Convolutional Generative Models. In *2019 IEEE/CVF Conference on Computer Vision and Pattern Recognition (CVPR)*, pages 6175–6183. IEEE, June 2019.
- [34] Olaf Ronneberger, Philipp Fischer, and Thomas Brox. U-Net: Convolutional Networks for Biomedical Image Segmentation. In *Medical Image Computing and Computer-Assisted Intervention – MICCAI 2015*, Lecture Notes in Computer Science, pages 234–241. Springer International Publishing, 2015.
- [35] Jascha Sohl-Dickstein, Eric Weiss, Niru Maheswaranathan, and Surya Ganguli. Deep Unsupervised Learning using Nonequilibrium Thermodynamics. In *Proceedings of the 32nd International Conference on Machine Learning*, pages 2256–2265. PMLR, June 2015.
- [36] Jiaming Song, Chenlin Meng, and Stefano Ermon. Denoising Diffusion Implicit Models. In *International Conference on Learning Representations*, October 2020.
- [37] Yang Song and Stefano Ermon. Generative Modeling by Estimating Gradients of the Data Distribution. In *Advances in Neural Information Processing Systems*, volume 32. Curran Associates, Inc., 2019.
- [38] Yang Song and Stefano Ermon. Improved Techniques for Training Score-Based Generative Models. In *Advances in Neural Information Processing Systems*, volume 33, pages 12438–12448. Curran Associates, Inc., 2020.
- [39] Yang Song, Jascha Sohl-Dickstein, Diederik P. Kingma, Abhishek Kumar, Stefano Ermon, and Ben Poole. Score-Based Generative Modeling through Stochastic Differential Equations. In *International Conference on Learning Representations*, 2021.
- [40] Jerry O. Talton, Yu Lou, Steve Lesser, Jared Duke, Radomír Měch, and Vladlen Koltun. Metropolis procedural modeling. *ACM Transactions on Graphics*, 30(2):11:1–11:14, April 2011.
- [41] Jiapeng Tang, Yinyu Nie, Lev Markhasin, Angela Dai, Justus Thies, and Matthias Nießner. DiffuScene: Scene Graph Denoising Diffusion Probabilistic Model for Generative Indoor Scene Synthesis. In *2024 IEEE/CVF Conference on Computer Vision and Pattern Recognition (CVPR)*, 2024.
- [42] Ashish Vaswani, Noam Shazeer, Niki Parmar, Jakob Uszkoreit, Llion Jones, Aidan N Gomez, Łukasz Kaiser, and Illia Polosukhin. Attention is All you Need. In *Advances in Neural Information Processing Systems*, volume 30. Curran Associates, Inc., 2017.
- [43] Kai Wang, Yu-An Lin, Ben Weissmann, Manolis Savva, Angel X. Chang, and Daniel Ritchie. PlanIT: planning and instantiating indoor scenes with relation graph and spatial prior networks. *ACM Transactions on Graphics*, 38(4):1–15, August 2019.
- [44] Xinpeng Wang, Chandan Yeshwanth, and Matthias Niesner. SceneFormer: Indoor Scene Generation with Transformers. In *2021 International Conference on 3D Vision (3DV)*, pages 106–115, London, United Kingdom, December 2021. IEEE.
- [45] Michael L. Waskom. seaborn: statistical data visualization. *Journal of Open Source Software*, 6(60):3021, 2021.
- [46] Qiuhong Anna Wei, Sijie Ding, Jeong Joon Park, Rahul Sajjani, Adrien Poulénard, Srinath Sridhar, and Leonidas Guibas. LEGO-Net: Learning Regular Rearrangements of Objects in Rooms. In *2023 IEEE/CVF Conference on Computer Vision and Pattern Recognition (CVPR)*, pages 19037–19047, Vancouver, BC, Canada, June 2023. IEEE.
- [47] Haitao Yang, Zaiwei Zhang, Siming Yan, Haibin Huang, Chongyang Ma, Yi Zheng, Chandrajit Bajaj, and Qixing Huang. Scene Synthesis via Uncertainty-Driven Attribute Synchronization. In *2021 IEEE/CVF International Conference on Computer Vision (ICCV)*, pages 5610–5620. IEEE, 2021.
- [48] Ming-Jia Yang, Yu-Xiao Guo, Bin Zhou, and Xin Tong. Indoor Scene Generation from a Collection of Semantic-Segmented Depth Images. In *2021 IEEE/CVF International Conference on Computer Vision (ICCV)*, pages 15183–15192, Montreal, QC, Canada, October 2021. IEEE.
- [49] Yi-Ting Yeh, Lingfeng Yang, Matthew Watson, Noah D. Goodman, and Pat Hanrahan. Synthesizing open worlds with constraints using locally annealed reversible jump MCMC. *ACM Transactions on Graphics*, 31(4):56:1–56:11, July 2012.

- [50] Lap-Fai Yu, Sai-Kit Yeung, Chi-Keung Tang, Demetri Terzopoulos, Tony F. Chan, and Stanley J. Osher. Make it home: automatic optimization of furniture arrangement. *ACM Transactions on Graphics*, 30(4):86:1–86:12, July 2011.
- [51] Lap-Fai Yu, Sai-Kit Yeung, and Demetri Terzopoulos. The Clutterpalette: An Interactive Tool for Detailing Indoor Scenes. *IEEE Transactions on Visualization and Computer Graphics*, 22(2):1138–1148, February 2016.
- [52] Guangyao Zhai, Evin Pınar Örnek, Shun-Cheng Wu, Yan Di, Federico Tombari, Nassir Navab, and Benjamin Busam. CommonScenes: Generating Commonsense 3D Indoor Scenes with Scene Graphs, October 2023.
- [53] Zaiwei Zhang, Zhenpei Yang, Chongyang Ma, Linjie Luo, Alexander Huth, Etienne Vouga, and Qixing Huang. Deep Generative Modeling for Scene Synthesis via Hybrid Representations. *ACM Transactions on Graphics*, 39(2):1–21, April 2020.
- [54] Yang Zhou, Zachary White, and Evangelos Kalogerakis. SceneGraphNet: Neural Message Passing for 3D Indoor Scene Augmentation. In *2019 IEEE/CVF International Conference on Computer Vision (ICCV)*, pages 7383–7391. IEEE, October 2019.
- [55] Yi Zhou, Connelly Barnes, Jingwan Lu, Jimei Yang, and Hao Li. On the Continuity of Rotation Representations in Neural Networks. In *2019 IEEE/CVF Conference on Computer Vision and Pattern Recognition (CVPR)*, pages 5738–5746. IEEE, June 2019.

A Diffusion Models

A.1 DDPM forward process re-parameterization, simplified loss

DDPM [15] suggests re-parameterizing Eq. (4) as

$$\mathbf{x}_t(\mathbf{x}_0, \epsilon) = \sqrt{\bar{\alpha}_t}\mathbf{x}_0 + \sqrt{1 - \bar{\alpha}_t}\epsilon \quad (16)$$

with $\epsilon \sim \mathcal{N}(\mathbf{0}, \mathbf{I})$. Then, let ϵ_θ be a function approximator to predict ϵ from \mathbf{x}_t such that for the reverse process $\mu_\theta(\mathbf{x}_t, t) = \frac{1}{\sqrt{\alpha_t}} \left(\mathbf{x}_t - \frac{\beta_t}{\sqrt{1 - \bar{\alpha}_t}} \epsilon_\theta(\mathbf{x}_t, t) \right)$ and L_{t-1} for $2 \leq t \leq T$ in (2) becomes

$$L_{t-1} = \mathbb{E}_{\mathbf{x}_0, \epsilon} \left[\frac{\beta_t^2}{2\sigma_t^2 \alpha_t (1 - \bar{\alpha}_t)} \left\| \epsilon - \epsilon_\theta(\sqrt{\bar{\alpha}_t}\mathbf{x}_0 + \sqrt{1 - \bar{\alpha}_t}\epsilon, t) \right\|^2 \right] + \text{const} \quad (17)$$

where the constant term can be dropped in training.

On image data, [15] found it beneficial to sample quality to train on this simplified version of the variational bound ($L_{0:T-1}$):

$$L_{\text{simple}}(\theta) := \mathbb{E}_{t, \mathbf{x}_0, \epsilon} \left[\left\| \epsilon - \epsilon_\theta(\sqrt{\bar{\alpha}_t}\mathbf{x}_0 + \sqrt{1 - \bar{\alpha}_t}\epsilon, t) \right\|^2 \right] \quad (18)$$

with uniform t between 1 and T , dropping the scaling factors of the squared norms. We use Eq. (18) to compute L_{vb}^{DDPM} in MiDiffusion.

A.2 D3PM reverse parameterization, auxiliary loss

Similar DDPM, [2, 16] suggested that approximating some surrogate variables gives better quality. Specifically, they trained a neural network $\tilde{p}_\theta(\tilde{z}_0|z_t)$, multiplied it with the posterior $q(z_{t-1}|z_t, z_0)$, and marginalized \tilde{z}_0 to obtain $p_\theta(z_{t-1}|z_t)$:

$$p_\theta(z_{t-1}|z_t) \propto \sum_{\tilde{z}_0} q(z_{t-1}|z_t, z_0) \tilde{p}_\theta(\tilde{z}_0|z_t). \quad (19)$$

D3PM [2] introduced an auxiliary denoising objective to encourage good predictions of the data z_0 at each time step. Their complete training loss is:

$$L_\lambda(\theta) = L_{vb}(\theta) + \lambda \mathbb{E}_{q(z_0)q(z_t|z_0)} [-\log \tilde{p}_\theta(z_0|z_t)] \quad (20)$$

which correspond to L_{vb}^{D3PM} and λL_{aux}^{D3PM} in our MiDiffusion algorithm. This can be implemented efficiently in training, since the parameterization of the backward step directly computes $\tilde{p}_\theta(z_0|z_t)$.

B MiDiffusion Loss Factorization

We provide more details for the factorization step in Eq. (13). We first consider a general case comparing KL-divergence between $\tilde{q}(z)\hat{q}(\mathbf{x})$ and $\tilde{p}(z)\hat{p}(\mathbf{x})$ for discrete z and continuous \mathbf{x} :

$$\begin{aligned} D_{\text{KL}}(\tilde{q}(z)\hat{q}(\mathbf{x})||\tilde{p}(z)\hat{p}(\mathbf{x})) &= \int_{\mathbf{x}} \sum_z \tilde{q}(z)\hat{q}(\mathbf{x}) \log \frac{\tilde{q}(z)\hat{q}(\mathbf{x})}{\tilde{p}(z)\hat{p}(\mathbf{x})} \\ &= \int_{\mathbf{x}} \sum_z \left[\tilde{q}(z)\hat{q}(\mathbf{x}) \log \frac{\tilde{q}(z)}{\tilde{p}(z)} + \tilde{q}(z)\hat{q}(\mathbf{x}) \log \frac{\hat{q}(\mathbf{x})}{\hat{p}(\mathbf{x})} \right] \\ &= \sum_z \tilde{q}(z) \log \frac{\tilde{q}(z)}{\tilde{p}(z)} \underbrace{\int_{\mathbf{x}} \hat{q}(\mathbf{x})}_{1} + \int_{\mathbf{x}} \hat{q}(\mathbf{x}) \log \frac{\hat{q}(\mathbf{x})}{\hat{p}(\mathbf{x})} \underbrace{\sum_z \tilde{q}(z)}_1 \\ &= D_{\text{KL}}(\tilde{q}(z)||\tilde{p}(z)) + D_{\text{KL}}(\hat{q}(\mathbf{x})||\hat{p}(\mathbf{x})). \end{aligned} \quad (21)$$

This means we can decouple KL-divergence computation between mixed-domain probability distributions to a sum of domain-specific KL-divergence computation. Note that this holds for any choices

of \tilde{q} , \hat{q} , \tilde{p} , \hat{p} . For our specific case:

$$\begin{aligned}
& L_{t-1}^{mixed} \\
&= \mathbb{E}_{q(z_t, \mathbf{x}_t | z_0, \mathbf{x}_0)} [D_{\text{KL}}(q(z_{t-1}, \mathbf{x}_{t-1} | z_t, \mathbf{x}_t, z_0, \mathbf{x}_0) || p_\theta(z_{t-1}, \mathbf{x}_{t-1} | z_t, \mathbf{x}_t, \mathbf{y})))] \\
&= \mathbb{E}_{\tilde{q}(z_t | z_0) \hat{q}(\mathbf{x}_t | \mathbf{x}_0)} [D_{\text{KL}}(\tilde{q}(z_{t-1} | z_t, z_0) \hat{q}(\mathbf{x}_{t-1} | \mathbf{x}_t, \mathbf{x}_0) || \tilde{p}_\theta(z_{t-1} | z_t, \mathbf{x}_t, \mathbf{y}) \hat{p}_\theta(\mathbf{x}_{t-1} | \mathbf{x}_t, z_t, \mathbf{y})))] \\
&= \mathbb{E}_{\tilde{q}(z_t | z_0)} [D_{\text{KL}}(\tilde{q}(z_{t-1} | z_t, z_0) || \tilde{p}_\theta(z_{t-1} | z_t, \mathbf{x}_t, \mathbf{y})))] \\
&\quad + \mathbb{E}_{\hat{q}(\mathbf{x}_t | \mathbf{x}_0)} [D_{\text{KL}}(\hat{q}(\mathbf{x}_{t-1} | \mathbf{x}_t, \mathbf{x}_0) || \hat{p}_\theta(\mathbf{x}_{t-1} | \mathbf{x}_t, z_t, \mathbf{y}))],
\end{aligned} \tag{22}$$

where the last equality holds because of Eq. (21).

C Network and Implementation Details

We include detailed network hyper-parameters for our denoising network, and implementation for training. We plan to release our code and training configurations upon acceptance of this paper.

C.1 Network Hyper-parameters

The architecture of MiDiffusion has at its core a series of 8 transformer blocks using a hidden dimension of 512 with 8 heads and feed-forward layers with an internal dimension of 2048. Following [11], we use GELU [14] as nonlinearity. The semantic attributes are embedded in a learned vector of length 512, and the geometric attributes are mapped by a 3-layer MLP, with internal dimensions of [512, 1024], to a 512-dimensional space before being fed to the transformer decoder blocks. We extract floor plan features of dimension 64 using a 4-layer PointNet [31] with internal dimensions [64, 64, 512] as in LEGO-Net [46]. The conditional input is concatenated with the learned 64-dimensional index embedding. For baselines and ablation studies, we use the default ResNet-18 [12] image feature extractor proposed by ATISS [28] and also implemented by DiffuScene [41] to compute the 64-dimensional floor plan features from binary floor plan masks. The outputs of the transformer decoder are fed to two separate MLPs to decode the semantic and geometric predictions. The semantic feature decoder is a 1-layer MLP that produces a categorical distribution over z , and the geometric feature decoder is a 3-layer MLP with hidden dimensions [512, 1024], producing the 8-dimensional Gaussian mean for the geometric attributes \mathbf{x} .

C.2 Implementation

We set a fixed learning rate of $l_r = 2e^{-4}$ using the Adam optimizer, and a dropout ratio of 0.1 for multi-head attention and feed-forward layers in the transformer blocks. We train 50k epochs on the bedroom dataset with 0.5 learning rate decay every 10k epochs, and 100k epochs on the living and dining room datasets with 0.5 decay every 15k epochs. We use a linear schedule over 1000 diffusion steps for all noise parameters in the forward process. In the discrete domain α_t and γ_t range from $1 - 1e^{-5}$ to 0.99999 and from $9e^{-6}$ to 0.99999 respectively. In the continuous domain, β_t starts from $1e^{-4}$ at reaches 0.02. We train all our models on a single NVIDIA V100 GPU with under 8GB of GPU RAM usage. The training time range from around 20 hours on living and dining room datasets to about 36 hours on the bedroom dataset for a batch size of 128 scenes.

D Example Synthesized Layout Images

We use texture-less object rendering on white floor plan for quantitative evaluations, since floor and object textures affect the clarity of the results. The object labels are sorted in alphabetical order for each room type, and then the associated colors are evenly sampled along a circular path using Seaborn’s [45] “hls” color palette. We render top-down layout images using simple-3dviz [1] in accordance with prior works [28, 41]. We include examples of rendered images for three comparing approaches in Fig. 7, 8, 9 from the floor-conditioned scene synthesis experiment in Sec 2. Some ground-truth layouts include objects slightly out of boundary. This is a problem in the raw 3D-FRONT dataset. Therefore, we inflate the room boundary by 0.1m when counting number of out of boundary objects. The bedroom datasets is the easiest (less number of objects, smaller in room size, more training data) so that all comparing approaches can generate good predictions. On the harder living room and dining room datasets, MiDiffusion clearly outperforms the baselines by generating realistic geometric arrangements with desired symmetry and alignment between objects, while respecting the

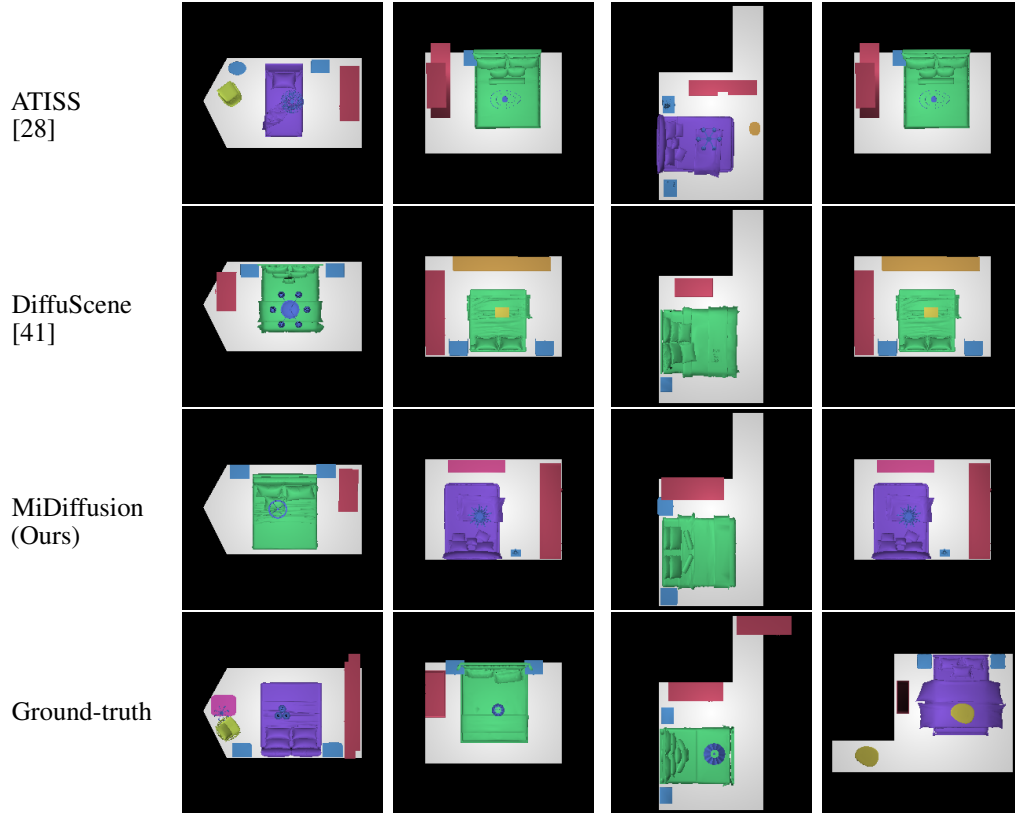


Figure 7: Example bedroom top-down orthographic projection images for quantitative evaluations.

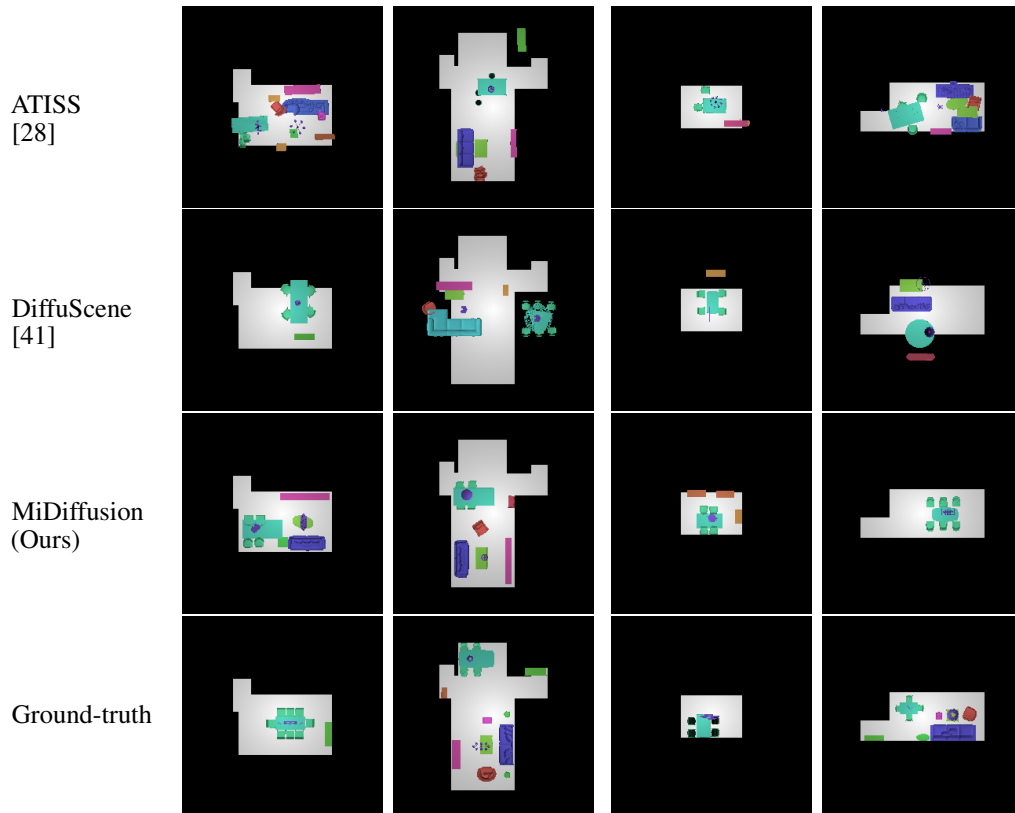


Figure 8: Example dining room top-down orthographic projection images for quantitative evaluations.

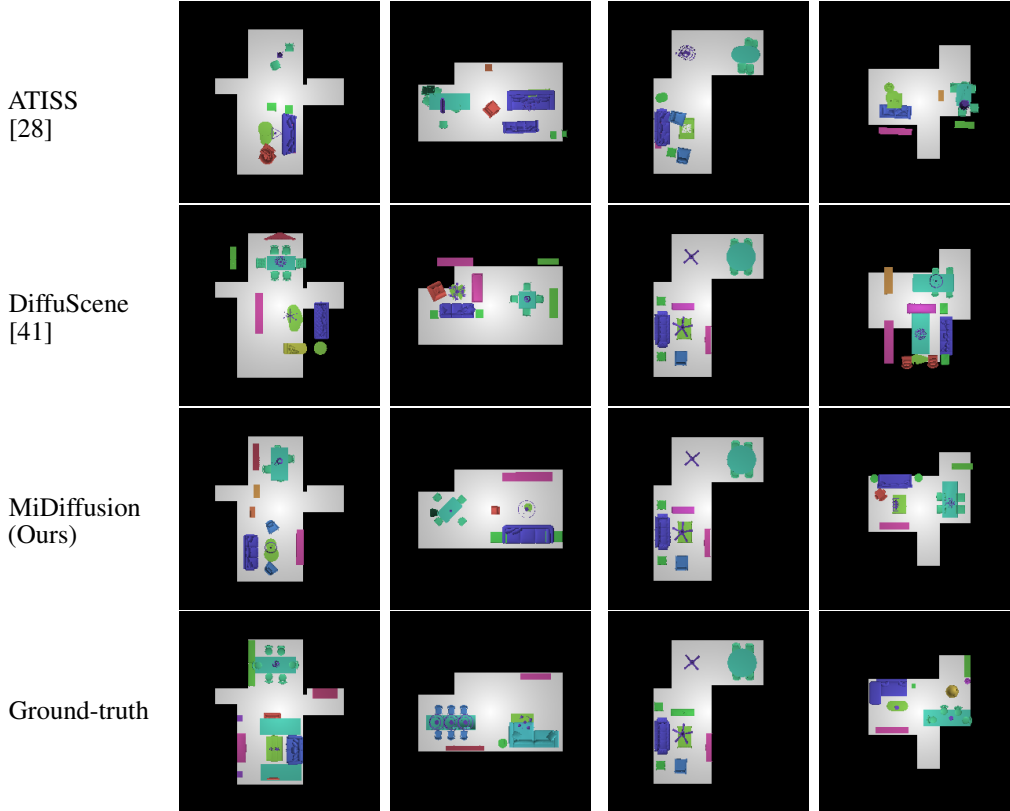


Figure 9: Example living room top-down orthographic projection images for quantitative evaluations.

floor boundary constraints. DiffuScene is also capable of generating good geometric arrangement but their architecture is less optimal for learning floor boundary constraints.

E Additional Experimental Evaluations

E.1 Ablation Study

We provide additional geometric evaluation results for our ablation study in Sec. 5.1. Across all three dataset, there is a consistent improvement over OOB % as we modify the floor plan feature extractor and diffusion framework towards our final design of MiDiffusion. This is consistent with the evaluation metrics reported in Sec. 5.1.

Method	Bedroom			Dining room			Living room		
	Obj	OOB %	IoU %	Obj	OOB %	IoU %	Obj	OOB %	IoU %
DDPM+ResNet	5.07	6.63	0.50	10.87	7.08	0.70	11.90	10.93	0.70
DDPM+PointNet	4.92	5.29	0.70	10.78	6.75	0.78	11.83	10.37	0.64
Mixed+PointNet	5.22	3.91	0.61	10.92	5.77	0.91	12.28	8.71	0.69
Ground truth	5.22	3.37	0.24	11.11	0.73	0.48	11.67	1.55	0.27

Table 7: Geometric evaluations on ablation study for floor-conditioned 3D scene synthesis.

E.2 Unconditional 3D Scene Synthesis

DiffuScene was originally proposed for 3D scene synthesis without floor conditioning. Although this is not the main focus of this paper, we provide experimental results comparing MiDiffusion and DiffuScene for completeness using the released model weights. DiffuScene used squares of the same size to render the layouts, which cuts off some objects in the dining and living rooms. We therefore re-compute DiffuScene results using their released models and render layouts to dataset specific sizes.

The results are summarized in Table 8. Our approach works better than DiffuScene on the dining room dataset, comparably on the living room dataset, and slightly worse on the bedroom dataset.

Table 9 shows results using DiffuScene’s default rendering and evaluation approach over the same set of results as Table 8. Specifically, we render all ground-truth and synthesized layouts to a 3.1m square. We compare the synthetic results with the ground-truth training set in accordance with DiffuScene’s evaluation script. We include the original results in [41] in the first row as a reference. Using pre-trained models and open-sourced evaluation scripts, we are able generate DiffuScene results close to publication values. The only exception is CA%, for which DiffuScene does not release their classification network. Therefore, we use the AlexNet [22] based classifier by ATISS [28]. These results are consistent with Table 8 that MiDiffusion behaves sub-optimally on the bedroom dataset. Our models are quite similar in performance compared to DiffuScene on dining room and living room datasets, even though they are not specifically designed for this task.

Method	Bedroom				Dining room				Living room			
	FID	KIDx0.001	CA %	KLx0.01	FID	KIDx0.001	CA %	KLx0.01	FID	KIDx0.001	CA %	KLx0.01
DiffuScene	61.12	0.46	53.70 ± 2.94	1.24	45.04	0.70	51.53 ± 1.05	1.10	43.30	0.21	53.50 ± 2.84	0.67
MiDiffusion (ours)	65.72	2.83	54.93 ± 3.85	1.12	43.61	0.42	51.21 ± 1.33	0.71	43.66	0.84	53.16 ± 2.32	0.61

Table 8: Evaluation results for unconditional 3D scene synthesis.

Method	Bedroom				Dining room				Living room			
	FID	KIDx0.001	CA %	KLx0.01	FID	KIDx0.001	CA %	KLx0.01	FID	KIDx0.001	CA %	KLx0.01
DiffuScene-[41]	17.21	0.70	52.15	0.35	32.60	0.72	55.50	0.22	36.18	0.88	57.81	0.21
DiffuScene	17.43	0.82	51.09 ± 0.47	0.66	33.07	0.93	53.82 ± 4.01	0.34	35.27	0.58	54.24 ± 3.65	0.36
MiDiffusion (Ours)	21.32	2.62	54.93 ± 3.85	0.32	33.05	0.87	52.32 ± 2.34	0.16	36.21	1.43	54.86 ± 2.59	0.16

Table 9: Evaluation results for unconditional 3D scene synthesis against training scenes and using layouts rendered on 3.1m squares.

F Additional Layout Examples

F.1 Qualitative Examples for Additional Applications

We show qualitative examples of additional applications of our models as explained in Sec. 5.2.3. Fig. 10 and 11 are two examples of label constrained scene synthesis. In particular, Fig. 11 is conditioned on five dining chairs, which occur less often than even number of chairs. Our model is still able to generate reasonable layout.

We show label constrained scene completion examples in Fig. 12 and Fig. 13. With our corruption-and-masking strategy, our models are able to complete scene layout under object category constraints.

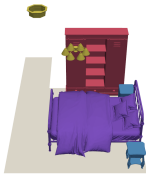


Figure 10: Label constrained bedroom scene synthesis.

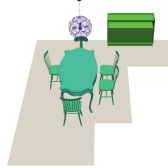


Figure 11: Label constrained dining room scene synthesis.

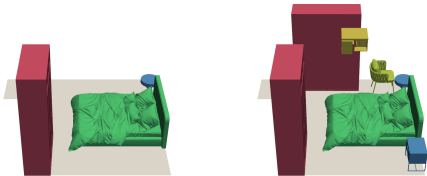


Figure 12: Label constrained bedroom scene completion.

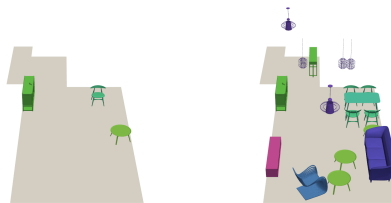


Figure 13: Label constrained living room scene completion.

F.2 Additional Layouts for Floor-Conditioned Scene Synthesis

We provide additional layout image generated by MiDiffusion in our floor-conditioned scene synthesis experiment. These layouts are generated in a sequence of random sampling of test floor plans after removing floor plan duplicates.

